Polytypism driven zero-field splitting of silicon vacancies in 6*H*-SiC

Timur Biktagirov,[1] Wolf Gero Schmidt,[1] Uwe Gerstmann,[1] Boris Yavkin,[2,3] Sergei Orlinskii,[2] Pavel Baranov,[4] Vladimir Dyakonov,[5] and Victor Soltamov[4,5]

[1]*Lehrstuhl für Theoretische Materialphysik, Universität Paderborn, 33098 Paderborn, Germany*

[2]*Kazan Federal University, 420008 Kazan, Russia*

[3]*3rd Institute of Physics, University of Stuttgart, 70569 Stuttgart, Germany*

[4]*Ioffe Institute, 194021 St. Petersburg, Russia*

[5]*Experimental Physics VI, Julius-Maximilian University of Würzburg, 97074 Würzburg, Germany*

(Received 2 August 2018; published 8 November 2018)

The fine-structure splitting in zero magnetic field allows one to access the coherent control and manipulation of polarized spin states. Here the zero-field splitting (ZFS) of the $S = 3/2$ silicon vacancy-related centers in 6*H*-SiC is explored by means of electron paramagnetic resonance and electron nuclear double resonance techniques, combined with first-principle calculations. We show that the centers not only possess significantly different absolute values of ZFS, but they also differ in their sign. This diversity is rationalized by a flattened/elongated character of their spin-density distribution, potentially alters spin-photon entanglement, and suggests these centers for qubits in the upcoming technology of quantum communication and quantum-information processing.

DOI: 10.1103/PhysRevB.98.195204

I. INTRODUCTION

Optical polarized spin states of color centers in solids appear to be an essential building block for modern quantum technologies (see Ref. [1] and references therein). Negatively charged silicon vacancies (V_{Si}^{-}) in SiC are prototypical examples in this context. They feature unique functionality for quantum sensing operated under ambient conditions [2,3], as well as for quantum communication using spin-photon entanglement [4]. They possess a high-spin $S = 3/2$ ground state [5,6], which splits into two Kramers doublets in zero-magnetic field. These doublets (either $M_S = \pm 3/2$ or $M_S = \pm 1/2$) can be optically polarized through an electron spin-dependent intersystem-crossing pathway and readout by means of optically detected magnetic resonance (ODMR) techniques [6,7]. Extremely long spin coherence times [8] combined with the ability of resonant optical addressing of the centers spin state at cryogenic temperatures [9] make these centers an ideal platform for quantum information processing.

However, for successful implementation in quantum technologies, a defect center has to simultaneously satisfy two requirements, namely high ODMR contrast and large enough splitting of the spin sublevels in zero magnetic field [10,11], both needed in order to gain efficient access to the spin. Recent studies show that in 4*H*-SiC there is a promising dichroic V_{Si}^{-} center [12], which features perfect properties at cryogenic temperatures (such as a Debye-Waller factor of 40% simultaneously with ODMR contrast close to 100%). However, for this particular center, the splitting of spin sublevels in zero magnetic field is only 4 MHz, which, according to Ref. [12], could become prohibitively too small for effective manipulation of the spin via radiofrequency (rf) fields. The polytypism of SiC, i.e., the ability to form many different crystal structures, appears as an additional lever to reach the ideal combination of magnetic and optical characteristics. Indeed, $S = 3/2$ silicon vacancy-related centers also exist in 6*H*-SiC, possessing intriguing properties [13–16]: They have at least the same ODMR contrast as in 4*H*, but also two of them show a sufficiently large zero-field splitting (ZFS or $2D$) equal to 28 and 128 MHz, depending on the lattice site [15]. This certainly suggests the 6*H* polytype as a host matrix for V_{Si}^{-}. However, while the influence of polytypism on the ZFS is obvious, its mechanism is essentially not understood.

Whereas the assignment of the $S = 3/2$ centers in 4*H*-SiC to isolated V_{Si}^{-} has been established in Ref. [16], there has been no conclusive analysis of the ZFS and their sign in the 6*H* polytype (see the supplemental material of Refs. [16,17]). Here, we explore the fine structure of the V_{Si}^{-} centers at inequivalent crystallographic sites of 6*H*-SiC by means of density functional theory (DFT) calculations as well as high-frequency electron paramagnetic resonance (EPR) and electron nuclear double resonance (ENDOR) techniques. We are able to show that one of these centers surprisingly exhibits a negative sign of D. This will have a crucial influence on future applications, since the sign change reflects the order of the Kramers doublets and thereby determines the protocol that has to be used to control a related spintronic device [4].

II. METHODS

DFT calculations were carried out using the QUANTUM ESPRESSO software [18,19] in order to correlate details of the spin distribution with a possible sign change in the D value. The defect structures were modeled with hexagonal 324-atom 6*H*-SiC supercells, for which the experimental lattice constants have been chosen [20] in order to diminish the influence of the used exchange-correlation functional. Norm-conserving pseudopotentials (generated with the Troullier-Martins approach [21]) and the PBE exchange-correlation

functional [22] were used with a plane-wave cutoff of 60 Ry. The defect structures were allowed to relax until the forces were less than 10^{-4} Ry/bohr. For the relaxed structures, evaluation of the spin-spin ZFS ($2D_{SS}$) was carried out with the recently reported implementation [23] into the GIPAW module of QUANTUM ESPRESSO. The convergence of the resulting D_{SS} values with respect to the level of Brillouin zone sampling was assured by using a shifted $2 \times 2 \times 2$ Monkhorst-Pack [24] k-point grid. For calculation of the electronic g tensor and the hyperfine (HF) splittings, the same settings were used.

Pulsed EPR and Mims-ENDOR [25] measurements were performed at W-band frequencies (≈ 94 GHz) by using the Bruker Elexsys 680 spectrometer. To produce V_{Si}^- centers, the 6H-SiC sample with a concentration of uncompensated nitrogen donors of 10^{15} cm^{-3} was irradiated with fast neutrons at room temperature with a dose of 10^{15}–10^{16} cm^{-2}.

III. RESULTS AND DISCUSSION

As the most important result of our calculations, we obtain a negative D_{SS} for one of the V_{Si}^- configurations [$V_{Si}^-(k1)$, cf. Table I]. This is a rather unusual observation for intrinsic defects in light-element semiconductors. However, a change of the sign of spin-spin ZFS upon structural alternation and flattened/elongated deformation of the spin density distribution is known in EPR spectroscopy of triplet-state organic molecules and is explained within the classical point-dipole approximation [26,27]. In SiC, it can be rationalized by the hexagonality of the 6H-SiC polytype (cf. Fig. 1), as will be discussed in the following.

The structure of 6H-SiC can be described by two quasicubic and one hexagonal Si-C double layer, which constitute a periodic sequence along the crystal c-axis of the unit cell providing three inequivalent crystallographic positions for the silicon vacancy: two quasicubic ($k1$ and $k2$) and one hexagonal (h) site. Irrespective of the site, the V_{Si}^- center exhibits C_{3v} symmetry and a high-spin $S = 3/2$ ground state ($^4A_2$) with three unpaired electrons distributed among the four carbon dangling bonds. However, as seen from Fig. 1, the presence of the hexagonal layers above and below the defect alters its coordination environment by introducing a twist of the lattice around the c-axis.

TABLE I. DFT calculated EPR parameters for the three inequivalent V_{Si}^- centers in 6H-SiC: g factor and the spin-spin ZFS parameter (D_{SS} in MHz) along with the experimental (D_{exp} in MHz) W-band values measured in this work (fourth column) and absolute values taken from Ref. [15] (last column).

	g factor	D_{SS}	D_{exp}	$\lvert D_{exp}\rvert$[a]
$V_{Si}^-(h)$	2.0031	5.9	0[b]	0
$V_{Si}^-(k1)$	2.0031	–30.4	–13.4	14
$V_{Si}^-(k2)$	2.0031	104.6	63.8	64

[a]Reference [15]. Assignment to certain lattice sites is based on our DFT results.
[b]Not resolved within the line shape of the central transition. An upper bound of ~1.5 MHz can be deduced.

It should be noted that in previous experimental works, the center with D equal to 64 MHz was tentatively associated with the h site, while D equal to 14 MHz was considered as a signature of both quasicubic sites ($k1$ and $k2$) [14,15]. The results of DFT calculations presented in Table I significantly refine the picture currently accepted to interpret the experimental data. First of all, we find that the $V_{Si}^-(k1)$ and $V_{Si}^-(k2)$ centers manifest very different D_{SS}. At the same time, the silicon vacancy at the h site is found to exhibit the smallest ZFS.

Detailed inspection of the HF parameters for the nearest-neighbor carbon (shell I) reveals that the structural differences

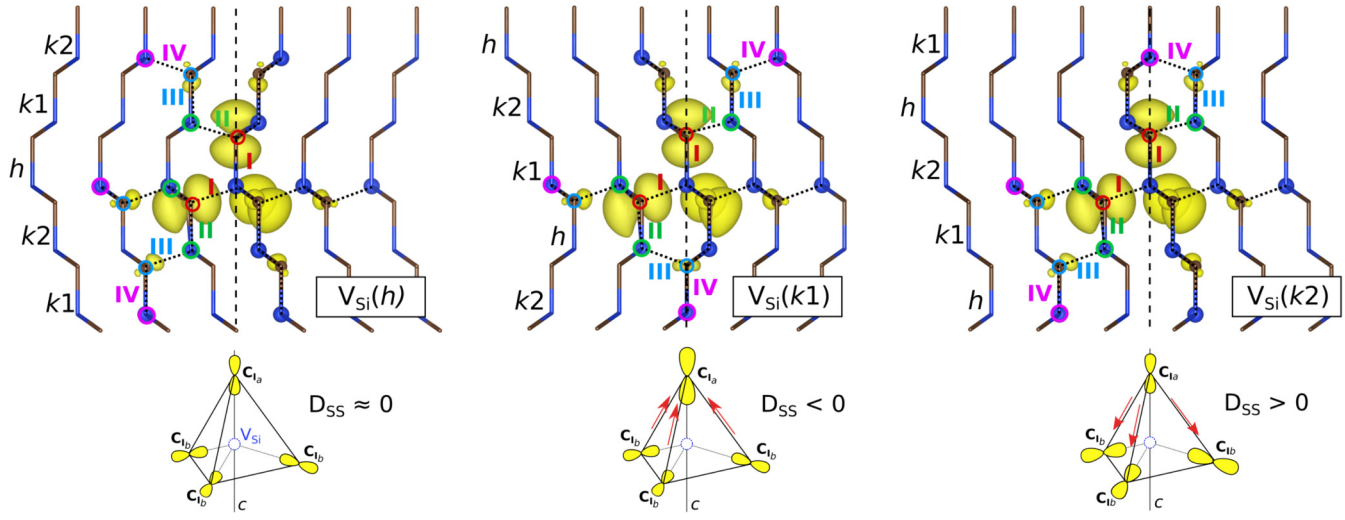

FIG. 1. Top: V_{Si}^- centers in 6H-SiC at the three inequivalent crystallographic sites: h, $k1$, and $k2$. The four coordination shells that exhibit the largest localization of spin density are marked with roman numbers I–IV. Selected atoms belonging to the shells are accordingly marked by colored circles. Yellow isosurfaces show the spin-density distribution. Vertical dashed lines indicate the c-axis of the defect, where considerable differences in the spin distribution can be found. Bottom: Schematic illustration of the flattening/elongation alternations in spin-density distribution leading to the different signs of D_{SS} [26,27], where the redistribution of the spin density is illustrated by the red arrows.

TABLE II. DFT calculated principal values (in MHz) of the HF interaction with axial (Ia) and basal (Ib) ^{13}C nuclei of the first coordination shell (i.e., the dangling bond C atoms) of the V_{Si}^- centers. As a measure of flattening of the spin-density distribution, a ratio $\eta = (A_\parallel^{Ib} - A_\parallel^{Ia})/A_\parallel^{Ib}$ is given ($\eta > 0$ for flattened and $\eta < 0$ for elongated character).

	$A_\parallel^{Ia}$	$A_\perp^{Ia}$	$A_\parallel^{Ib}$	$A_\perp^{Ib}$	η (%)
$V_{Si}^-(h)$	94.7	40.4	95.3	41.8	0.71
$V_{Si}^-(k1)$	96.2	41.7	91.8	37.9	–4.88
$V_{Si}^-(k2)$	93.3	42.7	97.1	41.9	3.92

between h, $k1$, and $k2$ sites induce slight but qualitatively distinct deformations of the electron distribution over the carbon dangling bonds (see Table II). For the $k2$ site, the more flattened character of the spin-density distribution is seen from Table II, which results in positive D_{SS} (cf. Table I). At the same time, the hexagonal layer below the $V_{Si}^-(k1)$ center promotes elongation of the spin system and by this a negative D_{SS} value. Notably, when the defect is located at the h site, it is surrounded by two cubic layers above and below. As a result, its spin density distribution mimics the perfectly symmetric case of the cubic 3C polytype up to the fourth coordination shell (with 12 quasiequivalent carbon atoms in shell III and 12 silicon atoms in shell IV). Consequently, a D_{SS} value comparatively close to zero is obtained. For this reason, a V_{Si}^- center with a vanishing ZFS value is not expected to be found in 4H-SiC [16], where, due to a higher degree of hexagonality (i.e., the ratio of the number of hexagonal layers to the total), such an arrangement does not appear.

To provide experimental confirmation for the predicted mechanism and to prove unambiguously the sign of D for the $k1$ or $k2$ configurations, pulsed EPR and Mims-ENDOR measurements were performed. First, we analyze the electron spin echo (ESE) detected EPR spectrum recorded with and without optical excitation ($\lambda_{exc} = 808$ nm) while applying a magnetic field parallel to the crystallographic c axis (Fig. 2). Under illumination, i.e., optical pumping of the Zeeman ground-state spin levels through an electron spin-dependent intersystem-crossing pathway [6,28], the fine-structure EPR transitions undergo phase reversal [Fig. 2(a)]. Furthermore, from the bottom inset of Fig. 2(a) it can be seen that, e.g., the high-field fine-structure components correspond to either $-3/2 \leftrightarrow -1/2$ (red arrow, $D > 0$) or $+1/2 \leftrightarrow +3/2$ (blue arrow, $D < 0$) spin transitions. With and without optical excitation, two pairs of fine-structure EPR transitions are observed with splittings ΔB equal to 9.1 and 1.9 mT. Based on the corresponding absolute D values of 63.8 and 13.4 MHz, they must thus be attributed to the negatively charged silicon vacancy at the quasicubic sites $V_{Si}^-(k1)$ and $V_{Si}^-(k2)$, respectively ($D = \gamma_e \Delta B/4$, where γ_e is the electron gyromagnetic ratio). The absolute D values coincide with previously reported X-band EPR/ODMR and zero-field ODMR data [13–16] (see also Table I). At the same time, the ZFS of the $V_{Si}^-(h)$ center is not resolved.

For the $V_{Si}^-(k2)$ center, the ESE-detected EPR spectrum measured at $T = 8$ K without optical excitation [see Fig. 2(b)] clearly reveals that the intensity of the high-field fine-structure

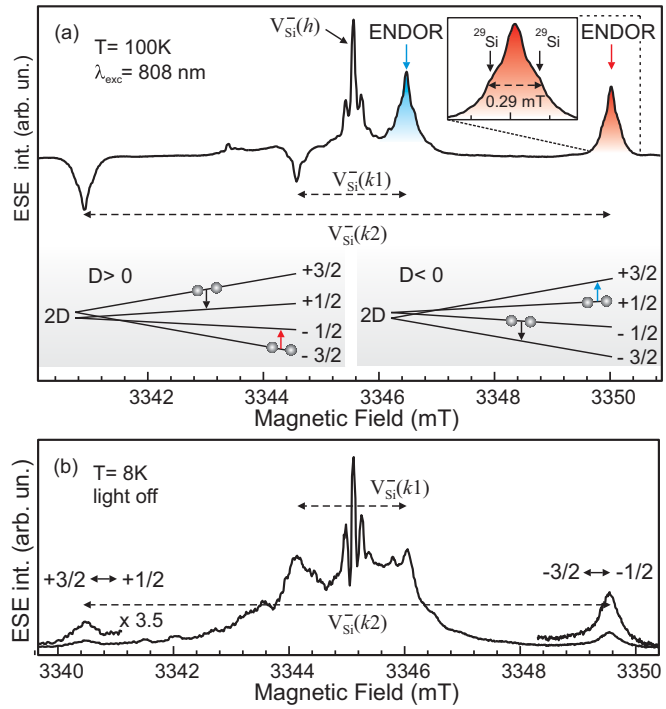

FIG. 2. (a) Optically induced W-band ESE spectrum of the 6H-SiC sample measured at $T = 100$ K for $\mathbf{B}\|\mathbf{c}$. Vertical colored arrows indicate the magnetic fields at which ENDOR spectra are measured. The top inset shows the HF structure due to the ^{29}Si nuclei from the II-d coordination shell (enlarged scale). The bottom inset illustrates the ZFS splitting and optically induced population inversion of the Zeeman levels, resulting in phase reversal of the fine-structure transitions depending on the sign of D. (b) W-band ESE spectrum ($\mathbf{B}\|\mathbf{c}$) now measured at $T = 8$ K in the dark. The M_S manifolds and respective EPR transitions (×3.5 enlarged) are labeled according to the diagrams in (a).

component is about three times larger than that of the low-field one. This intensity ratio agrees with the thermal populations of the Zeeman levels. Indeed, given the current experimental conditions ($T = 8$ K, $\nu \approx 94$ GHz), the Boltzmann population of the $M_S = +1/2$ level is roughly one-third of that of the lowest one [$M_S = -3/2$; cf. the energy level diagram in Fig. 2(a)]. Thereby, we can attribute the more intense high-field fine-structure component to the $-3/2 \leftrightarrow -1/2$ transition and deduce the positive D for $V_{Si}^-(k2)$. However, from Fig. 2(b) it becomes clear that such an assignment for the $V_{Si}^-(k1)$ center is not conclusively possible due to the partial overlap of its spectrum with other EPR spectroscopic features of the sample.

To overcome this obstacle, we make use of the ^{29}Si ENDOR spectra. Here, the transitions ($\Delta M_S = 0$, $\Delta M_I = \pm 1$) obey frequencies $\nu_{ENDOR} = |\nu_L + AM_S|$, where the Larmor frequency for ^{29}Si nuclei (with negative nuclear g factor, $g_n = -1.110\,58$) is defined as $\nu_L = \mu_n |g_n| B/h$ [29,30]. This equation shows the direct relation between the ENDOR-frequency splitting for a given HF coupling constant, A, and the electron spin sublevel, M_S, to which this splitting corresponds. Thereby, one can unambiguously deduce the EPR transition for which the ENDOR spectrum is recorded, if the sign of A is known, and vice versa.

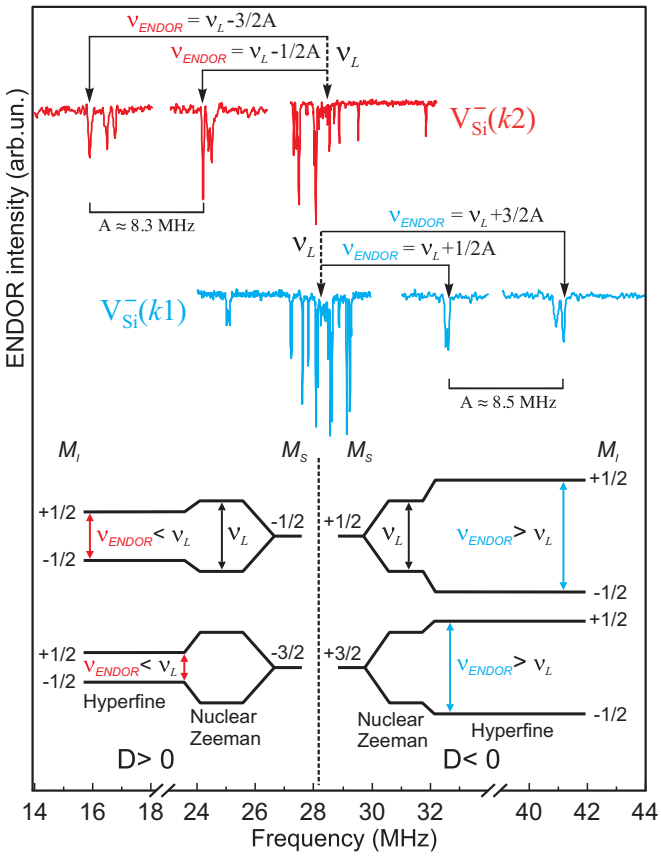

FIG. 3. Mims-ENDOR spectra selectively measured on the fine-structure EPR lines of the $V_{Si}^-(k2)$ (top) and the $V_{Si}^-(k1)$ (middle). ^{29}Si Larmor frequencies, ν_L, are indicated by arrows. Horizontal bars indicate the splitting of ENDOR frequencies corresponding to the HF interaction with ^{29}Si nuclei in the II-d coordination shell. Note that no further HF transitions related to this coordination shell can be observed in the ENDOR spectra (cf. diagrams in the bottom inset and discussion in the text). Other ENDOR splittings observed in the vicinity of ν_L can be assigned to the ^{29}Si nuclei of more distant coordination shells. The spectra are measured at $T = 100$ K under illumination ($\lambda_{exc} = 808$ nm). The energy level diagram for $S = 3/2$, $I = 1/2$ (bottom) illustrates the dependence of the ENDOR frequencies $\nu_{ENDOR} = |\nu_L + AM_S|$ on the sign of the D value, whereby a positive HF splitting, A, is taken into account.

The ENDOR spectra presented in Fig. 3 are selectively measured at magnetic field positions of the high-field fine-structure transitions of the $V_{Si}^-(k1)$ and $V_{Si}^-(k2)$ EPR signals [cf. Fig. 2(a)]. The spectra then only contain nuclear frequencies of two M_S manifolds: for $V_{Si}^-(k2)$ it is $-1/2$ and $-3/2$, whereas for $V_{Si}^-(k1)$ it has to be deduced. One can readily see that the overall HF splitting pattern of $V_{Si}^-(k1)$ is mirrored with respect to ν_L in comparison to that of $V_{Si}^-(k2)$. From Fig. 3 it becomes thus immediately obvious that the $V_{Si}^-(k1)$ and the $V_{Si}^-(k2)$ centers exhibit a different sign of D.

This is especially conspicuous for the HF coupling with the nuclei of 12 Si atoms in the II-d coordination shell. This HF splitting is known to be almost independent of the position of V_{Si}^- within the lattice (see Refs. [16,17]). It is isotropic with a positive value of about 8 MHz [16,17,31], showing that at these ^{29}Si nuclei with a negative nuclear g_n factor the minority spin ("down") is locally dominant. In the case of $V_{Si}^-(k2)$, cf. Fig. 3 (top spectrum), the corresponding HF-related transitions are found at frequencies *below* ν_L, i.e., on the left-hand side with respect to ν_L, confirming a positive D that results from a $-3/2 \leftrightarrow -1/2$ fine-structure transition. For the vacancy at the $k1$ site, the situation is the opposite. The characteristic ^{29}Si-related transitions are found on the right-hand side of ν_L, more precisely at $\nu_L + 1/2A$ and $\nu_L + 3/2A$; cf. Fig. 3 (bottom spectrum). We thus can attribute the high-field fine-structure component of the EPR spectrum of $V_{Si}^-(k1)$ to the $+1/2 \leftrightarrow +3/2$ electron spin transition, and the corresponding D is indeed negative.

IV. CONCLUSION

In this work, we have provided insight into the fine structure of the $S = 3/2$ silicon vacancy centers in 6H-SiC. In particular, all three inequivalent V_{Si}^- configurations are found to bear qualitatively different ZFS: The central result of our work is that one of the silicon vacancy configurations in 6H-SiC exhibits a negative fine-structure constant, in contrast to those in the 4H polytype. The surprising diversity of D in the V_{Si}^- centers can be explained by the hexagonality of SiC and its influence on the defect microscopic structure and electronic spin distribution.

The presence of V_{Si}^- centers with different signs of ZFS in the same host material is an important discovery, which directly affects the choice of protocols for future quantum technological applications. The order of the Kramers doublets in the ground state, $M_S = \pm 3/2$ or $M_S = \pm 1/2$, is, e.g., also crucial for a successful implementation into a spin-photon entanglement interface: Unlike $M_S = \pm 1/2$ states, the former cannot be directly connected via external fields, thus requiring the use of a different protocol for implementation of a Hadamard-like gate [4]. The insight in the defect fine structure obtained here is highly relevant in the context of recently reported progress in generation of the silicon-vacancy defects in predetermined locations [32], where entanglement schemes will make use of the coupling between the spin states of the nearest-neighbor defects. The details of the V_{Si}^- fine structure presented here open new avenues for application of silicon vacancies in the 6H and, potentially, in other higher index SiC polytypes.

ACKNOWLEDGMENTS

Numerical calculations were performed using grants of computer time from the Paderborn Center for Parallel Computing (PC^2) and the HLRS Stuttgart. The Deutsche Forschungsgemeinschaft (DFG) is acknowledged for financial support via the priority program SPP1601 (U.G., V.D.). EPR and ENDOR measurements were done at Kazan Federal University and financially supported by Russian Science Foundation (Project No. 17-72-20053, B.Y.). S.O. also acknowledges financial support of Program of Competitive Growth of KFU for upgrading the EPR spectrometer. P.B. was supported by the RFBR Project No. 16-02-00877. V.S. gratefully acknowledges the financial support of the Alexander von Humboldt (AvH) Foundation.

[1] M. Atatüre, D. Englund, N. Vamivakas, S.-Y. Lee, and J. Wrachtrup, Nat. Rev. Mater. **3**, 38 (2018).

[2] D. Simin, V. A. Soltamov, A. V. Poshakinskiy, A. N. Anisimov, R. A. Babunts, D. O. Tolmachev, E. N. Mokhov, M. Trupke, S. A. Tarasenko, A. Sperlich, P. G. Baranov, V. Dyakonov, and G. V. Astakhov, Phys. Rev. X **6**, 031014 (2016).

[3] S.-Y. Lee, M. Niethammer, and J. Wrachtrup, Phys. Rev. B **92**, 115201 (2015).

[4] S. E. Economou and P. Dev, Nanotechnology **27**, 504001 (2016).

[5] N. Mizuochi, S. Yamasaki, H. Takizawa, N. Morishita, T. Ohshima, H. Itoh, T. Umeda, and J. Isoya, Phys. Rev. B **72**, 235208 (2005).

[6] H. Kraus, V. A. Soltamov, D. Riedel, S. Väth, F. Fuchs, A. Sperlich, P. G. Baranov, V. Dyakonov, and G. V. Astakhov, Nat. Phys. **10**, 157 (2014).

[7] M. Widmann, S.-Y. Lee, T. Rendler, N. T. Son, H. Fedder, S. Paik, L.-P. Yang, N. Zhao, S. Yang, I. Booker, A. Denisenko, M. Jamali, S. A. Momenzadeh, I. Gerhardt, T. Ohshima, A. Gali, E. Janzén, and J. Wrachtrup, Nat. Mater. **14**, 164 (2015).

[8] D. Simin, H. Kraus, A. Sperlich, T. Ohshima, G. V. Astakhov, and V. Dyakonov, Phys. Rev. B **95**, 161201(R) (2017).

[9] D. Riedel, F. Fuchs, H. Kraus, S. Väth, A. Sperlich, V. Dyakonov, A. A. Soltamova, P. G. Baranov, V. A. Ilyin, and G. V. Astakhov, Phys. Rev. Lett. **109**, 226402 (2012).

[10] D. DiVincenzo, Nat. Mater. **9**, 468 (2010).

[11] J. R. Weber, W. F. Koehl, J. B. Varley, A. Janotti, B. B. Buckley, C. G. Van de Walle, and D. D. Awschalom, Proc. Natl. Acad. Sci. USA **107**, 8513 (2010).

[12] R. Nagy, M. Widmann, M. Niethammer, D. B. R. Dasari, I. Gerhardt, Ö. O. Soykal, M. Radulaski, T. Ohshima, J. Vúcković, N. T. Son, I. G. Ivanov, S. E. Economou, C. Bonato, S. Y. Lee, and J. Wrachtrup, Phys. Rev. Appl. **9**, 034022 (2018).

[13] H. J. von Bardeleben, J. L. Cantin, I. Vickridge, and G. Battistig, Phys. Rev. B **62**, 10126 (2000).

[14] E. Sorman, N. T. Son, W. M. Chen, O. Kordina, C. Hallin, and E. Janzen, Phys. Rev. B **61**, 2613 (2000).

[15] P. G. Baranov, A. P. Bundakova, A. A. Soltamova, S. B. Orlinskii, I. V. Borovykh, R. Zondervan, R. Verberk, and J. Schmidt, Phys. Rev. B **83**, 125203 (2011).

[16] V. Ivády, J. Davidsson, N. T. Son, T. Ohshima, I. A. Abrikosov, and A. Gali, Phys. Rev. B **96**, 161114 (2017).

[17] V. Ivády, J. Davidsson, N. T. Son, T. Ohshima, I. A. Abrikosov, and A. Gali, Mater. Sci. Forum **924**, 895 (2018).

[18] P. Giannozzi, O. Andreussi, T. Brumme, O. Bunau *et al.*, J. Phys.: Condens. Matter **29**, 465901 (2017).

[19] P. Giannozzi, S. Baroni, N. Bonini, M. Calandra *et al.*, J. Phys.: Condens. Matter **21**, 395502 (2009).

[20] A. Bauer, J. Kräußlich, L. Dressler, P. Kuschnerus, J. Wolf, K. Goetz, P. Käckell, J. Furthmüller, and F. Bechstedt, Phys. Rev. B **57**, 2647 (1998).

[21] N. Troullier and J. L. Martins, Phys. Rev. B **43**, 1993 (1991).

[22] J. P. Perdew, K. Burke, and M. Ernzerhof, Phys. Rev. Lett. **77**, 3865 (1996).

[23] T. Biktagirov, W. G. Schmidt, and U. Gerstmann, Phys. Rev. B **97**, 115135 (2018).

[24] H. J. Monkhorst and J. D. Pack, Phys. Rev. B **13**, 5188 (1976).

[25] W. B. Mims, Proc. R. Soc. London, Ser. A **283**, 452 (1965).

[26] S. Richert, C. E. Tait, and C. R. Timmel, J. Magn. Res. **280**, 103 (2017).

[27] P. J. Angiolillo, V. S.-Y. Lin, J. M. Vanderkooi, and M. J. Therien, J. Am. Chem. Soc. **117**, 12514 (1995).

[28] Ö. O. Soykal, P. Dev, and S. E. Economou, Phys. Rev. B **93**, 081207(R) (2016).

[29] J. A. Weil and J. R. Bolton, *Electron Paramagnetic Resonance* (Wiley, New York, 2007).

[30] P. G. Baranov, H. J. von Bardeleben, F. Jelezko, and J. Wrachtrup, *Magnetic Resonance of Semiconductors and Their Nanostructures* (Springer-Verlag, Wien, 2017).

[31] T. Wimbauer, B. K. Meyer, A. Hofstaetter, A. Scharmann, and H. Overhof, Phys. Rev. B **56**, 7384 (1997).

[32] J. Wang, Y. Zhou, X. Zhang, F. Liu, Y. Li, K. Li, Z. Liu, G. Wang, and W. Gao, Phys. Rev. Appl. **7**, 064021 (2017).